Phase Transitions of Nonlinear Waves in Quadratic Waveguide Arrays

Frank Setzpfandt,[1,2] Andrey A. Sukhorukov,[2] Dragomir N. Neshev,[2] Roland Schiek,[1,3] Yuri S. Kivshar,[2] and Thomas Pertsch[1]

[1]*Friedrich-Schiller-University Jena, Max-Wien-Platz 1, 07743 Jena, Germany*

[2]*Nonlinear Physics Center, Research School of Physics and Engineering, Australian National University, Canberra, 0200 ACT, Australia*

[3]*University of Applied Sciences Regensburg, Prüfeninger Strasse 58, 93049 Regensburg, Germany*

(Received 29 June 2010; published 1 December 2010)

We study two-color parametric nonlinear modes in waveguide arrays with a quadratic nonlinear response. We predict theoretically and observe experimentally a new type of phase transition manifested in an abrupt power-controlled change of the mode structure from unstaggered to staggered, due to the interplay of localization and synchronization in parametrically driven discrete systems.

DOI: 10.1103/PhysRevLett.105.233905 PACS numbers: 42.65.Ky, 42.25.Fx

Synchronization of oscillations and wave localization are two fundamental nonlinear phenomena that have been driving the field of nonlinear dynamics for decades. Synchronization and phase locking [1] are known to exist in systems of different physical origin due to external driving and coupling between elements. Examples include the synchronous flashing of fireflies and the pulsation of laser arrays [2,3]. On the other hand, the localization of waves in nonlinear lattices, such as waveguide arrays, is also determined by coupling between the individual lattice sites [4]. As intersite coupling and nonlinearity govern the two phenomena, a natural question is if they can be linked together and what kind of novel fundamental effects can arise due to their interplay.

In this Letter, we reveal a new type of phase transition in nonlinear lattices occurring due to the interplay of localization and synchronization. We expect that this phenomenon can appear in various physical contexts, and we demonstrate its occurrence in optics where we obtain experimental evidence of the effect by directly monitoring laser beam reshaping. Specifically, we consider laser beam propagation through an array of closely spaced optical waveguides in media with quadratic nonlinearity that facilitates frequency conversion and energy exchange between the fundamental wave (FW) and second-harmonic (SH) beams. In such structures, the SH dynamics is governed by two mechanisms of energy exchange [Fig. 1(a)]: (i) an effective driving force by the FW [5] at the same lattice site and (ii) direct coupling of SH waves between the lattice sites due to the overlap of the neighboring waveguide modes. We show that each of these mechanisms could lead to synchronization of SH dynamics and formation of different phase patterns. Mechanism (i) is dominant when the FW (and the corresponding effective driving force) extends over many lattice sites, whereas mechanism (ii) dominates when the FW exhibits nonlinear self-trapping to a single lattice site. We specially design our experimental conditions to observe this interplay, overcoming for the first time the constraint of all previous experiments where the second mechanism was suppressed due to the inhibition of linear coupling for the SH modes [4]. The key observation of our work is that as the optical power is increased and the beam becomes more localized, the output beam profile at the second harmonic exhibits a sharp transformation from in-phase (unstaggered) to out-of-phase (staggered) patterns between the neighboring waveguides. We show that the effect of such a phase

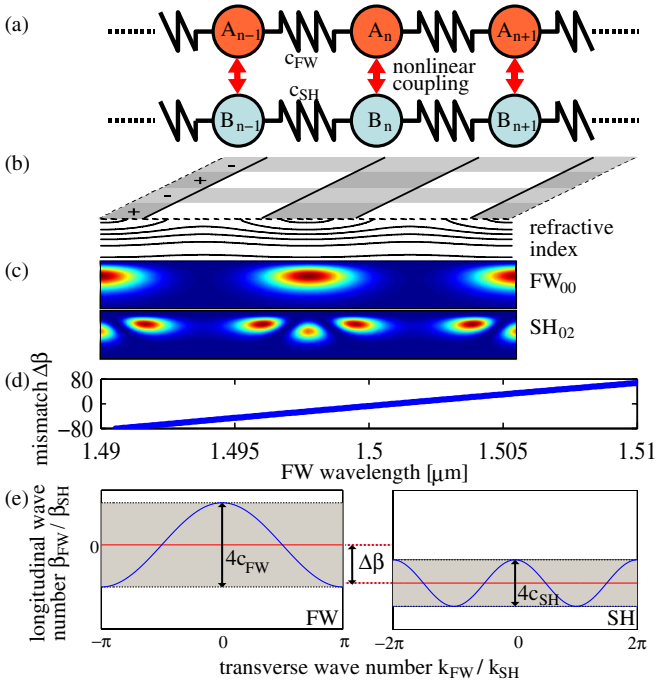

FIG. 1 (color online). (a) Scheme of the investigated system. (b) Sketch of the periodically poled lithium niobate sample depicting the refractive index profile. (c) Intensity profiles of the FW and SH modes. (d) Phase mismatch dependence on the FW wavelength. (e) Dispersion relations of the FW (left) and SH (right) modes.

transition on the output beam profile can be gradually adjusted simply by shifting the position of the input beam with respect to the lattice. These results demonstrate a generic phenomenon of localization-controlled phase locking, which opens up new possibilities for manipulating oscillations in nonlinear systems, including all-optical phase control of beams in photonic structures.

We study beam dynamics in an array of coupled waveguides in periodically poled lithium niobate [Fig. 1(b)] that features strong quadratic nonlinear response. To demonstrate the existence of a phase transition, we explore the nonlinear interaction between the FW_{00} and SH_{02} modes, whose intensity profiles are shown in Fig. 1(c). Both of these modes show linear coupling of comparable strength. This is in contrast to all previous experiments that utilized the nonlinear interaction between FW_{00} and SH_{00} but with negligible linear coupling of the SH_{00} modes due to their strong localization. The spatial beam evolution in such arrays can be modeled by a system of normalized equations for the mode amplitudes at the individual waveguides [4]:

$$\begin{aligned} &id_z A_n + c_{\mathrm{FW}}(A_{n+1} + A_{n-1}) + A_n^* B_n = 0, \\ &id_z B_n + c_{\mathrm{SH}}(B_{n+1} + B_{n-1}) - \Delta\beta B_n + A_n^2 = 0. \end{aligned} \tag{1}$$

Here z is the propagation distance normalized to z_s, d_z denotes the derivative with respect to the propagation direction, and A_n and B_n are the normalized FW and SH mode amplitudes in the nth waveguide, respectively. Note that the total power in the array $P = P_{\mathrm{FW}} + P_{\mathrm{SH}}$ is conserved, where $P_{\mathrm{FW}} = \sum_n |A_n|^2$ and $P_{\mathrm{SH}} = \sum_n |B_n|^2$. The real coefficients $c_{\mathrm{FW,SH}} = z_s \pi/(2L^c_{\mathrm{FW,SH}})$ determine the coupling strength between the neighboring waveguides, where $L^c_{\mathrm{FW,SH}}$ are the physical coupling lengths. The phase mismatch between the FW and SH waves (accounting for the periodic poling) is characterized by the value of $\Delta\beta$. Tuning-curve measurements show that $\Delta\beta$ depends on the FW frequency as shown in Fig. 1(d).

In the linear regime the beam dynamics is governed by the dispersion relations for the Bloch modes of the lattice [6]: $A_n(z) = A_0(z=0)\exp(ik_{\mathrm{FW}}n + i\beta_{\mathrm{FW}}z)$ for the FW and $B_n(z) = B_0(z=0)\exp(ik_{\mathrm{SH}}n + i\beta_{\mathrm{SH}}z)$ for the SH. Here $\beta_{\mathrm{FW}} = 2c_{\mathrm{FW}}\cos(k_{\mathrm{FW}})$ and $\beta_{\mathrm{SH}} = 2c_{\mathrm{SH}}\cos(k_{\mathrm{SH}}) - \Delta\beta$. Characteristic dispersion relations are schematically shown in Fig. 1(e). For propagation constants outside the shaded bands, the linear waves exhibit evanescent decay due to the photonic band gap [7]: $A_n = \kappa_1^{-|n|}$ and $B_n = \kappa_2^{-|n|}$, where $\kappa_j = [1 + (1 - \eta_j^2)^{1/2}]/\eta_j$ with $\eta_1 = 2c_{\mathrm{FW}}/\beta_{\mathrm{FW}}$ and $\eta_2 = 2c_{\mathrm{SH}}/(\beta_{\mathrm{SH}} + \Delta\beta)$. We note that for propagation constants below the bands ($\beta_{\mathrm{FW}} < -2c_{\mathrm{FW}}$ and $\beta_{\mathrm{SH}} < -2c_{\mathrm{SH}} - \Delta\beta$), $\kappa_j < 0$; i.e., the evanescent waves are staggered, with π phase oscillations between neighboring waveguides.

Next, we demonstrate that nonlinear parametric coupling of FW and SH waves can modify the phase pattern of the propagating waves. We note that most efficient SH generation occurs when the waves are spatially localized, due to enhanced local field intensities. Stronger localization occurs at higher optical powers due to self-focusing.

In order to reveal the generic relation between the nonlinear localization and phase locking, we first analyze the stationary localized states or fixed points of the system. Their power dependence provides insight into the bifurcation properties, revealing possible phase transitions. These solutions have the form $A_n(z) = A_n(z=0)\exp(i\beta z)$ and $B_n(z) = B_n(z=0)\exp(2i\beta z)$ [4,8]. Here β is a real parameter, which simultaneously defines the FW ($\beta_{\mathrm{FW}} = \beta$) and SH ($\beta_{\mathrm{SH}} = 2\beta$) propagation constants due to nonlinear synchronization. By substituting these expressions into Eqs. (1), we obtain a set of nonlinear equations for the real amplitudes of FW and SH. Whereas the solutions of these equations can be found only numerically, we identify the phase transition effect analytically by analyzing the tails of localized states, where $|A_n| \to 0$ and $|B_n| \to 0$ for $|n| \gg 0$. The solution for the FW tail is the same as for linear evanescent waves: $A_n \approx \kappa_1^{-|n|}$. For the SH wave, the nonlinear term representing the effective FW driving force cannot be neglected even in the small-amplitude limit. We perform asymptotic analysis and derive asymptotic expressions for the SH beam tails: $B_n \approx \kappa_2^{-|n|}$ if $|\kappa_2| < \kappa_1^2$ and $B_n \approx (\kappa_1^2)^{-|n|}$ if $|\kappa_2| > \kappa_1^2$. In the first case, the SH tail profile corresponds to a linear evanescent wave solution, whereas in the second case the SH tail is fully determined by the FW. A nontrivial phase transformation occurs when the propagation constant is below the bands, $\beta < \beta_1 = \min(-2c_{\mathrm{FW}}, -c_{\mathrm{SH}} - \Delta\beta/2)$, since in this case $\kappa_j < 0$. While the FW tails are always staggered, the SH tail exhibits a phase transition at

$$\beta_{s\pm} = -c_{\mathrm{FW}}^2 c_{\mathrm{SH}}^{-1} \pm \sqrt{c_{\mathrm{FW}}^4 c_{\mathrm{SH}}^{-2} + 2c_{\mathrm{FW}}^2 - \Delta\beta c_{\mathrm{FW}}^2 c_{\mathrm{SH}}^{-1}}. \tag{2}$$

The SH tails are staggered for $\beta < \beta_{s-}$ and $\beta > \beta_{s+}$ and unstaggered for $\beta_{s-} < \beta < \beta_{s+}$. Importantly, for weak or zero coupling of the SH mode ($c_{\mathrm{SH}} \simeq 0$), $\beta_{s\pm}$ diverges and no phase transition is present. Therefore, in all previous experiments with quadratic waveguide arrays, no such phase transition could be observed. Under our experimental conditions, the coupling lengths are practically constant in the frequency range around $\Delta\beta = 0$, with values $L^c_{\mathrm{SH}} \simeq L^c_{\mathrm{FW}} \simeq 20$ mm. By choosing the scaling coefficient $z_s = 2L^c_{\mathrm{FW}}/\pi$, the corresponding normalized coupling constants are $c_{\mathrm{FW,SH}} \simeq 1$.

The SH structure in the center and in the tails of the solutions can be different. Figure 2(a) presents the numerically calculated parameter regions for odd-type solutions (centered on a lattice site [4,8]), where the boundaries for phase transitions in the tails and for the entire soliton are indicated. Figures 2(b) and 2(c) show the intensity and phase profiles of the odd-type solutions vs β for $\Delta\beta = 1$. For low absolute values of β, the FW component of the solution is staggered and the SH component is unstaggered. If the value of β is decreased below β_{s-}, the FW component becomes very narrow. Hence the SH is driven only at a

few waveguides and becomes independent of the FW component. Here the SH component undergoes a *phase transition* to the staggered state. Such a transition has never been shown before, although soliton solutions with staggered-staggered and staggered-unstaggered FW and SH components have been reported [7–9]. Unambiguous signatures of the phase transition are observed in the spatial Fourier spectrum [Fig. 2(d)]. While the FW spectrum is always confined around the edge of the Brillouin zone ($k_{\mathrm{FW}} \simeq \pm\pi$), the SH Fourier spectrum switches between the center and the edge of the Brillouin zone, corresponding to a transition from an unstaggered to a staggered profile. It is relevant to note that, while multicolor discrete staggered solitons have been observed for polychromatic light [10], no phase transition of the localized states was present due to the incoherent coupling of the spectral components. Thus, the phase transition predicted here is a unique feature appearing due to the parametric process and the energy exchange between spectral components.

Figure 2(e) shows the soliton power corresponding to Figs. 2(b)–2(d). The monotonic dependence of the power on the propagation constant is generic for all soliton families exhibiting the phase transition, since they all bifurcate from the FW band edge. Such solitons are stable [8]. For values of the propagation constant below the phase transition threshold, the SH power of the solution is much smaller than the FW power [Fig. 2(f)], and indeed in this regime the SH is fully driven by the FW.

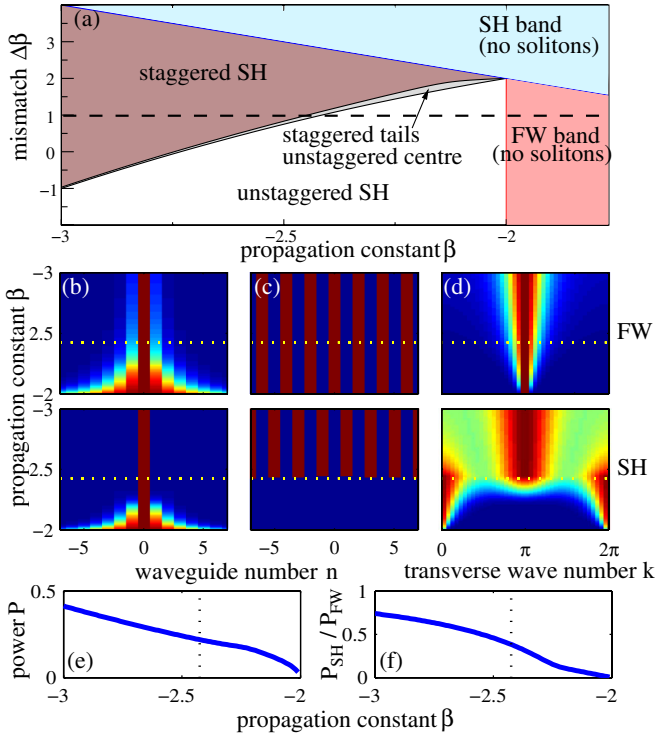

FIG. 2 (color online). (a) Regions of existence and different topologies of the odd soliton solutions with $c_{\mathrm{FW}} = c_{\mathrm{SH}} = 1$. (b)–(f) Soliton families for $\Delta\beta = 1$ [indicated by the dashed line in (a)]: (b) absolute values of the mode amplitudes, (c) phases where blue corresponds to 0 and red to π. (d) Absolute values of the spatial Fourier spectra. (e) Total power and (f) power ratio $P_{\mathrm{SH}}/P_{\mathrm{FW}}$. The dotted lines in (b)–(f) mark $\beta_{s\pm}$ where the SH tail profiles exhibit a phase transition.

We also analyze even-type solutions, where the FW profile is centered between neighboring lattice sites [4,8]. We find that, similar to the odd solutions, a phase transition occurs for the SH tails; see Fig. 3. However, the SH amplitudes at the two central sites are forced to have the same phase due to the even symmetry. Accordingly, the energy is always concentrated in the center of the Brillouin zone [Fig. 3(c)]. This demonstrates the possibility to partially suppress the phase transition. Although the even solitons exhibit symmetry-breaking instability and tend to transform to odd solitons [8], we confirm below that the instability develops relatively slowly such that the even symmetry is preserved in the experiments.

Next we study the predicted phase transition experimentally. In our experiments, only the FW beam is launched into the structure, leading to dynamical reshaping involving generation of SH and focusing. Nevertheless, the key predictions based on the analysis of stationary solutions are fully confirmed. We excite the array with 5.2 ps pulses generated by a tunable optical parametric amplifier at FW wavelengths around 1500 nm. The beam is shaped into an elliptic input beam with a horizontal (vertical) FWHM of 63 (2.8) μm. To obtain the staggered FW profile, the beam is tilted at the Bragg angle. The input power, controlled with a half-wave plate and a polarizer, is monitored before coupling to the sample. The array consists of 101 parallel waveguides with a pitch of 15 μm, made by titanium indiffusion in a 71-mm-long periodically poled lithium niobate crystal [11]. The sample is contained in an oven and heated to 220 °C to prevent photorefractive effects. After the sample, the powers of the transmitted FW and the generated SH components are measured and their intensity distributions are recorded by an InGaAs and a CCD camera, respectively. To obtain the spatial Fourier spectrum of the SH, we employ a lens and an additional CCD camera.

The upper row of Fig. 4 shows results of the power-dependent measurement of the SH Fourier spectrum for different phase mismatches, as determined by the input wavelength in accordance with Fig. 1(d). For low input

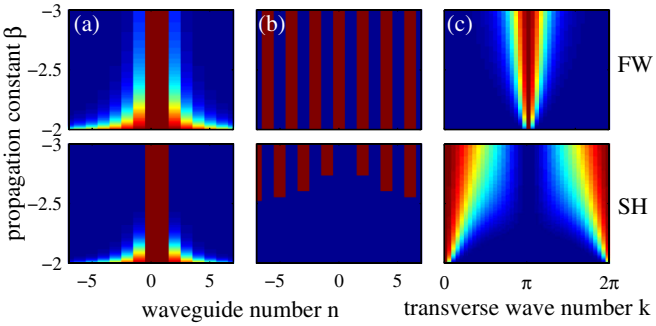

FIG. 3 (color online). Soliton families with even symmetry: (a) mode amplitudes, (b) phases, and (c) Fourier spectra. Notations and parameters correspond to Figs. 2(b)–2(d).

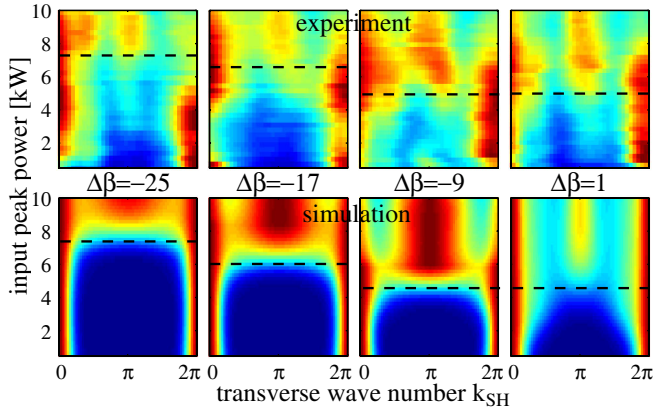

FIG. 4 (color online). Experimental (upper row) and numerical (bottom row) power dependence of the SH spatial output spectrum for different normalized mismatches $\Delta\beta$. The dashed lines mark the transition powers.

powers, the SH Fourier spectrum is concentrated around $k_{\mathrm{SH}} = 0, 2\pi$, corresponding to unstaggered SH. For FW input powers above a mismatch-dependent threshold, staggered SH components are generated at $k_{\mathrm{SH}} = \pi$. This is an unambiguous signature of the localization-controlled phase transition, as found for the stationary states.

To validate the interpretation of the experimental results and to explain possible differences to the stationary case, we also carry out simulations of the time-dependent coupled mode equations including group velocity mismatch and pulse dispersion [12]. The simulation results are plotted in the bottom row of Fig. 4 and agree well with the measured data. Measured and simulated FW peak power thresholds for a phase transition of the SH show a decrease from 7.5 kW for $\Delta\beta = -25$ to 5.5 kW for $\Delta\beta = 1$. In contrast to the predictions for stationary solutions, the SH transformation is not complete, since the wings of the pulse remain in their initial state. Thus we always measure nonzero SH powers at $k_{\mathrm{SH}} = 0, 2\pi$.

Another remarkable feature found in the stationary solutions is the absence of the complete phase transition for even symmetry (see Fig. 3). Figure 5(a) shows a set of experimental results for different transverse shifts of the sample with respect to the broad input beam. The SH

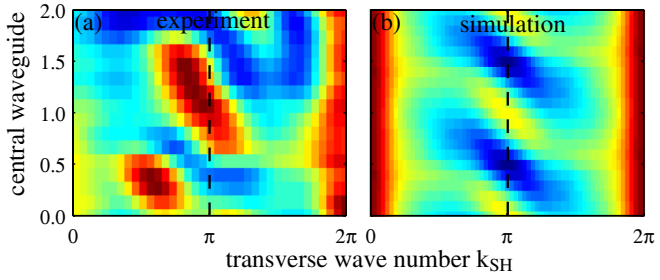

FIG. 5 (color online). (a) Experimental and (b) numerical dependencies of the SH spatial spectrum on the center of the excitation for $\Delta\beta = -9$ and an input peak power of 10 kW. The dashed line marks $k_{\mathrm{SH}} = \pi$.

spectral power at $k_{\mathrm{SH}} = \pi$ depends strongly on the position of the input beam. When the excitation is centered on a waveguide (odd), staggered SH is generated according to Fig. 4. For even excitation, centered between two waveguides, the SH power at $k_{\mathrm{SH}} = \pi$ vanishes. This shows that the symmetry dependence of the phase transition found in the stationary solution is a robust generic property. The comparison with the time-dependent simulations [Fig. 5(b)] again shows good agreement. Deviations between measurements and simulations are due to sample and input coupling inhomogeneities as well as to the general restrictions of the coupled mode equations.

In conclusion, we have predicted theoretically and demonstrated experimentally an abrupt power-controlled change of the SH field structure in quadratic nonlinear waveguide arrays from unstaggered to staggered phase profiles. The demonstrated effect of a symmetry-controlled phase transition offers great flexibility for tailoring phase structures, which may be further extended to other types of localized solutions, including twisted and vortex states [4,13]. The observed localization-induced phase transition is a generic phenomenon, and we anticipate that it can also occur in other nonlinear discrete systems such as Bose-Einstein condensates on optical lattices and gene networks in living cells [14].

The authors thank W. Sohler for sample preparation. This work was supported by the Deutsche Forschungsgemeinschaft (Research Unit 532 "Nonlinear spatial-temporal dynamics in dissipative and discrete optical systems"), the Federal Ministry of Education and Research (Innoregio-ZIK), and the Australian Research Council.

[1] A. Pikovsky, M. Rosenblum, and J. Kurths, *Synchronization: A Universal Concept in Nonlinear Sciences* (Cambridge University Press, Cambridge, England, 2003), p. 432.
[2] A. T. Winfree, Science **298**, 2336 (2002).
[3] L. Larger and J. M. Dudley, Nature (London) **465**, 41 (2010).
[4] F. Lederer *et al.*, Phys. Rep. **463**, 1 (2008).
[5] S. M. Saltiel, A. A. Sukhorukov, and Yu. S. Kivshar, Prog. Opt. **47**, 1 (2005).
[6] T. Pertsch *et al.*, Phys. Rev. Lett. **88**, 093901 (2002).
[7] A. A. Sukhorukov *et al.*, Phys. Rev. E **63**, 016615 (2000).
[8] T. Peschel, U. Peschel, and F. Lederer, Phys. Rev. E **57**, 1127 (1998).
[9] M. I. Molina, R. A. Vicencio, and Yu. S. Kivshar, Phys. Rev. E **72**, 036622 (2005).
[10] A. A. Sukhorukov, D. N. Neshev, and Yu. S. Kivshar, Opt. Express **15**, 13 058 (2007).
[11] R. Iwanow *et al.*, Opto-Electron. Rev. **13**, 113 (2005).
[12] R. Iwanow *et al.*, Phys. Rev. Lett. **93**, 113902 (2004).
[13] Z. Y. Xu and A. A. Sukhorukov, Opt. Lett. **34**, 1168 (2009).
[14] D. McMillen *et al.*, Proc. Natl. Acad. Sci. U.S.A. **99**, 679 (2002).